Check for updates

Lessons Learned From Modeling Irrigation From Field to Regional Scales

Xiaoyu Xu[1,2] (iD), Fei Chen[3] (iD), Michael Barlage[3] (iD), David Gochis[3] (iD), Shiguang Miao[2] (iD), and Shuanghe Shen[1]

[1]Collaborative Innovation Center on Forecast and Evaluation of Meteorological Disasters, Nanjing University of Information Science and Technology, Nanjing, China, [2]Institute of Urban Meteorology, China Meteorological Administration, Beijing, China, [3]National Center for Atmospheric Research, Boulder, CO, USA

Abstract Correctly calculating the timing and amount of crop irrigation is crucial for capturing irrigation effects on surface water and energy budgets and land-atmosphere interactions. This study incorporated a dynamic irrigation scheme into the Noah with multiparameterization land surface model and investigated three methods of determining crop growing season length by agriculture management data. The irrigation scheme was assessed at field scales using observations from two contrasting (irrigated and rainfed) AmeriFlux sites near Mead, Nebraska. Results show that crop-specific growing-season length helped capture the first application timing and total irrigation amount, especially for soybeans. With a calibrated soil-moisture triggering threshold (IRR_CRI), using planting and harvesting dates alone could reasonably predict the first application for maize. For soybeans, additional constraints on growing season were required to correct an early bias in the first modeled application. Realistic leaf area index input was essential for identifying the leaf area index-based growing season. When transitioning from field to regional scales, the county-level calibrated IRR_CRI helped mitigate overestimated (underestimated) total irrigation amount in southeastern Nebraska (lower Mississippi River Basin). In these two heavily irrigated regions, irrigation produced a cooling effect of 0.8–1.4 K, a moistening effect of 1.2–2.4 g/kg, a reduction in sensible heat flux by 60–105 W/m^2, and an increase in latent heat flux by 75–120 W/m^2. Most of irrigation water was used to increase soil moisture and evaporation, rather than runoff. Lacking regional-scale irrigation timing and crop-specific parameters makes transferring the evaluation and parameter-constraint methods from field to regional scales difficult.

1. Introduction

Irrigated agriculture applied on ~20% of global croplands contributes to ~40% of the world's food production (Siebert & Döll, 2010), which consumes about 70% of global total freshwater withdrawals and constitutes the largest share (~90%) of consumptive water use (Food and Agriculture Organization, 2010). In the United States, about 55.8 million acres of farmland were irrigated in 2012 and the irrigation withdrawals were 115 billion gallons per day (Maupin et al., 2014). Facing increased demand for food and water and the adverse climate impacts on water availability (Schewe et al., 2014; Vörösmarty et al., 2000), it is imperative to advance the understanding of the human-perturbed agriculture-water-climate interactions for addressing challenges such as food security and water scarcity in sustainable ways.

Observations (e.g., Bonfils & Lobell, 2007; Chen et al., 2018; Mahmood et al., 2006) and model simulations (e.g., Boucher et al., 2004; de Rosnay et al., 2003; Haddeland et al., 2006; Kueppers et al., 2007; Leng et al., 2013; Ozdogan et al., 2010; Pokhrel et al., 2012; Sacks et al., 2009) have demonstrated the important role of irrigation in modifying land surface water and energy budgets and subsequently local and regional weather and climate. For instance, irrigation reduced near-surface air temperature by decreasing (increasing) surface sensible (latent) heat fluxes (e.g., Chen et al., 2018; Cook et al., 2015; Haddeland et al., 2006; Leng et al., 2013; Ozdogan et al., 2010; Pei et al., 2016; Qian et al., 2013; Sacks et al., 2009). Wetter soils and higher latent heat fluxes led to higher atmospheric water vapor (Boucher et al., 2004), which in turn could enhance cloud cover and downwind precipitation (Cook et al., 2015; Pei et al., 2016; Qian et al., 2013). At large scales, the irrigation effects were more complicated as a result of interactions among multiscale atmospheric and land processes (Pei et al., 2016). For example, extensive

irrigation over the Indian peninsula delayed the South Asia summer monsoon onset and weakened the monsoon flow by reducing land-sea thermal contrasts, leading to less oceanic moisture transport and a redistribution and/or reduction of summer rainfall (e.g., Cook et al., 2015; Douglas et al., 2009; Guimberteau et al., 2012; Lee et al., 2011; Puma & Cook, 2010; Saeed et al., 2009; Shukla et al., 2014; Tuinenburg et al., 2014).

Applying a realistic irrigation scheme is important for obtaining a more reliable and quantitative estimate of the irrigation effects on climate (Sorooshian et al., 2011). Recent irrigation modeling in climate models shows significant discrepancies in the magnitudes of cooling or moistening induced by irrigation (e.g., Boucher et al., 2004; Lobell et al., 2006; Sacks et al., 2009). To a large degree, such discrepancies are related to how the irrigation models determine the irrigation water amount and timing. Some studies used available estimates of the evapotranspiration flux due to irrigation (e.g., Boucher et al., 2004) or the daily/annual irrigation amount (e.g., Cook et al., 2015; Lee et al., 2011; Puma & Cook, 2010; Sacks et al., 2009; Shukla et al., 2014) from earlier reports (e.g., Döll & Siebert, 2002; Wisser et al., 2010) as model input. Some other studies set the root-zone soil moisture (SM) over irrigated tiles to a critical value (e.g., soil saturation or field capacity) at every time step, year round (e.g., Kueppers et al., 2007; Lobell et al., 2009; Saeed et al., 2009; Tuinenburg et al., 2014), resulting in overestimations in modeled irrigation water amounts.

Recently, more complex irrigation parameterizations have been incorporated into various host land surface models (LSMs; Nazemi & Wheater, 2015; Pokhrel et al., 2016; McDermid et al., 2017), by using the "SM deficit" approach to dynamically represent irrigation implementations. For example, Ozdogan et al. (2010) checked three trigger criteria daily at 0600 local time (LT), that is, irrigated tile, growing season (defined by a threshold of 40% of annual range of greenness fraction), and root-zone SM availability (SMA) and computed the irrigation water demand by subtracting the current root-zone SM from field capacity (i.e., "SM deficit"). The extent of irrigated regions was identified by using the Moderate Resolution Imaging Spectroradiometer (MODIS)-based irrigated fractional area map (~500 m; Ozdogan & Gutman, 2008) as model input to the Noah LSM (Chen et al., 1996). Leng et al. (2013) also considered irrigation applications for the C3 generic crop in the Community Land Model. But they defined the growing season with crop leaf area greater than zero and employed a deficit from target SM content (SMC) rather than field capacity in Ozdogan et al. (2010). Sorooshian et al. (2011, 2012, 2014) used a similar deficit algorithm and constrained irrigation applications with downward solar radiation less than 50 W/m^2 and soil temperature greater than 10°C.

There are two major deficiencies in the current approach to modeling irrigation: (1) prior studies evaluated models against the county-level total irrigation water withdrawals but rarely evaluated the timing of irrigation and modeled at field scales and (2) lack of systematic assessment of impacts of auxiliary input data on constraining model performance. Therefore, this study explored these issues by incorporating a dynamic irrigation scheme into the Noah with multiparameterization (Noah-MP) LSM (Niu et al., 2011) using numerous agriculture management data sets and evaluated it at both field and regional scales. The control and optimization of various irrigation-model parameters were also assessed when transitioning from field scales to continental scales.

The rest of this paper was organized as follows. Section 2 presented data and methodology, including field observations and regional agriculture management data for model input and verification, and the dynamic irrigation scheme. Section 3 focused on the model performance evaluation at field and regional scales and analyzed the influence of agriculture management data as well as model sensitivities to various irrigation parameters. Finally, conclusions and some discussions were provided in section 4.

2. Data, Model, and Methodology

2.1. Agriculture Management Data

Compared to previous irrigation modeling studies, one unique aspect of this study is to integrate diverse agriculture management data and explore their impacts on constraining model solutions. For instance, to determine the extent of irrigation, we used the 500-m MODIS-based global map of irrigation fraction (hereinafter F_{irr}; Ozdogan & Gutman, 2008), which has been validated against agricultural statistics at the state and
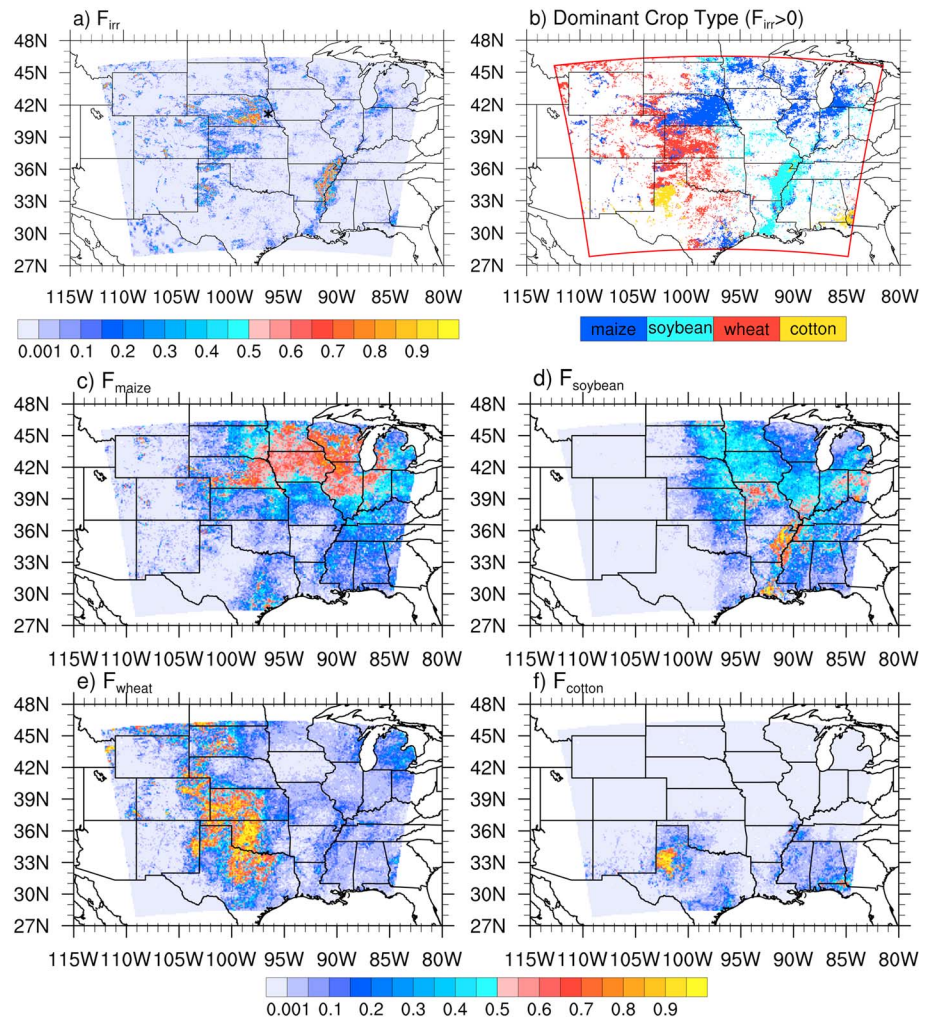
Figure 1. (a) The Moderate Resolution Imaging Spectroradiometer (MODIS)-based fractional area of irrigated lands. (b) Dominant crop type over irrigated grids. (c-f) The fractional coverage of each crop type (i.e., maize, soybean, winter wheat, and cotton).

county levels and widely used in modeling studies (e.g., Leng et al., 2013; Ozdogan et al., 2010; Qian et al., 2013). Figure 1a shows the fractional area of irrigated lands on the 4-km grid-spacing modeling domain used in this study. The choice of this modeling domain was somewhat arbitrary and aimed to include the Corn Belt in the Central Great Plains and croplands in the Lower Mississippi River Basin (LMRB) and to address the temperature warm-bias issue in convection-permitting regional climate modeling (Liu et al., 2017).

Irrigation applications are usually crop specific (McDermid et al., 2017), and each type of crop has distinct irrigation timing and water requirements. To capture such regional variability, this study used the following crop-specific agriculture management data to constrain the irrigation modeling:

1. Thirty-meter CropScape data from the U.S. Department of Agriculture's (USDA) National Agricultural Statistics Service (NASS)/George Mason University (https://nassgeodata.gmu.edu/CropScape/), which is a georeferenced, crop-specific land cover data layer created for the contiguous United States using satellite imagery and extensive agricultural ground truth. This dataset was used to calculate the fractional coverage of total cropland (relative to the grid cell's vegetated area; hereinafter F_{crop}) and of each crop type (relative to the grid cell's total cropland area; hereinafter F_{maize}, $F_{soybean}$, F_{wheat}, and F_{cotton}, see Figures 1c-1f).
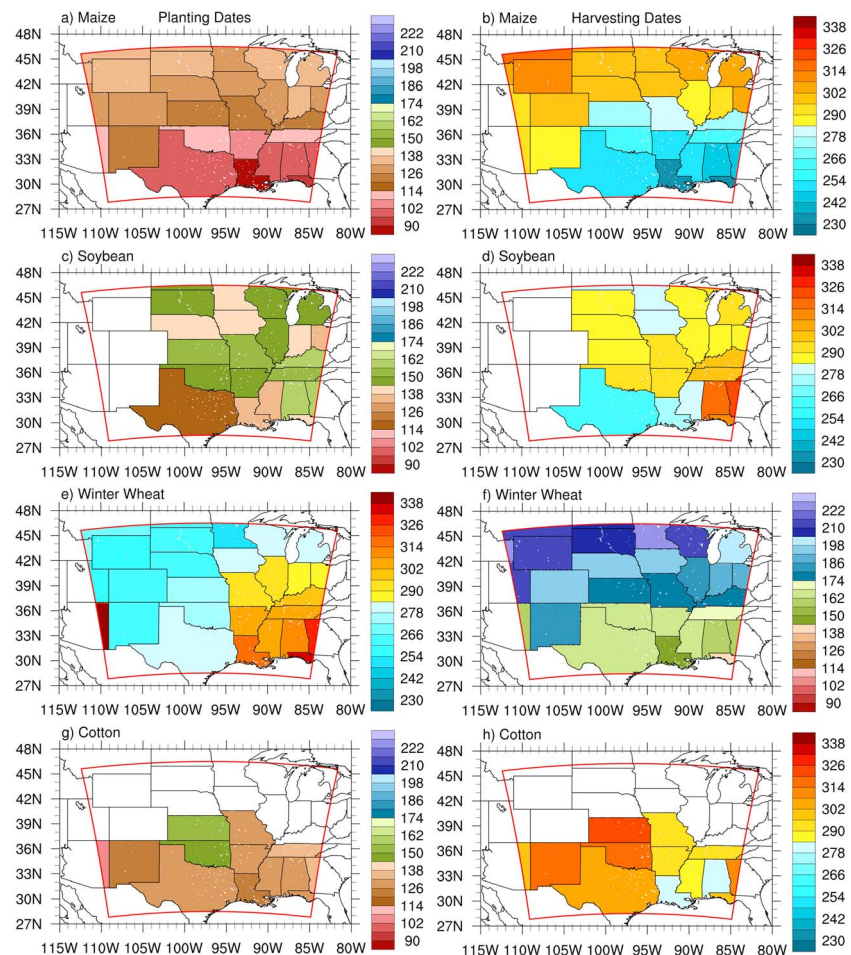
Figure 2. State-level maps of usual planting (left panels) and harvesting (right panels) dates (in Julian day format) for (a and b) maize, (c and d) soybean, (e and f) winter wheat, and (g and h) cotton.

2. USDA/NASS state-level maps of usual planting and harvesting dates, which indicate the periods in which the crops were planted or harvested in most years based on 20 years of historical crop progress estimates and the knowledge of industry specialists, for four major field crops (i.e., maize, soybean, winter wheat, and cotton). To be specific, this study employed the medium dates of NASS-reported "most active" ranges (National Agricultural Statistics Service, 2010) as model input planting and harvesting dates (see Figure 2), which indicate when between 15% and 85% of the crop is planted or harvested. Here, blank areas within the study domain (as shown by red lines in Figure 2) indicate no data due to the absence of the crop in those states (see Figures 1c-1f).

3. Global 1-km MODIS climatology leaf area index (LAI), which has been widely employed as input dataset for the Weather Research and Forecasting (WRF) model.

Table 1
Irrigation Scheme Parameters

Parameter	Description
IRR_CRI	irrigation trigger criterion, soil water availability percentage [0-1]
IRR_LIM	daily maximum amount to irrigate, mm
IRR_LAI	minimum LAI to trigger irrigation
IRR_GDD	minimum growing degree days to trigger irrigation, crop-specific
IRR_FRC	irrigation fraction above which to activate [0-1]
IRR_BEG	irrigation start time, local time
IRR_LEN	irrigation duration, hours
IRR_HAR	days before harvesting to stop irrigation
IRR_PCP	precipitation rate when irrigation stops, mm/hr

Abbreviations: GDD, growing degree day; LAI, leaf area index.

2.2. Irrigation Model Description

Numerical experiments for both field-scale and regional-scale were performed with the offline version of the Noah-MP LSM (Niu et al., 2011) running within the High-Resolution Land Data Assimilation System (HRLDAS v3.9; Chen et al., 2007). HRLDAS is a highly efficient and

parallelized LSM driver that can be executed for a single point (e.g., field-scale simulations) and for continental scales. It has evolved from a soil-state initialization tool to an efficient framework to test and evaluate the LSM (e.g., Gao et al., 2015; Li et al., 2018; Osuri et al., 2017; Xin et al., 2018; Zhang et al., 2016).

As a new development to Noah-MP, a dynamic irrigation scheme was incorporated, and Table 1 documents the various irrigation model parameters. Sprinklers are used on 68% of farms and irrigate 80% of the total farmland acreage in the Central Great Plains states (National Agricultural Statistics Service, 2009); so the irrigation scheme developed here mainly focused on sprinkler practice. For a given irrigation method (e.g., sprinkler considered in this study), the irrigation timing and amount are the two key aspects of irrigation modeling (Ozdogan et al., 2010). Here, the SM deficit approach was employed as a basic irrigation trigger as in previous studies (e.g., Leng et al., 2013; Ozdogan et al., 2010), but the growing season wherein irrigations were applied was defined in different ways with the inclusion of crop-specific management data. To simulate crop irrigation, each grid cell of the model was divided into irrigated (F_{irr}) and nonirrigated fractions according to 500-m MODIS-based irrigation fraction (Ozdogan & Gutman, 2008), and the area of irrigated cropland (hereinafter $F_{irr\text{-}crop}$) took the smaller value of F_{irr} and $F_{veg} \cdot F_{crop}$ (cropland fraction relative to the model grid cell's total area; Leng et al., 2013).

$$F_{irr\text{-}crop} = \min\left(F_{irr}, F_{crop} \cdot F_{veg}\right). \tag{1}$$

For the irrigated cropland tile, the root-zone SMA was defined as the ratio of the current root-zone available SM (defined as the difference to the wilting point SM_{wlt}) and nonstress SM (defined as the difference between field capacity (SM_{ref}) and SM_{wlt}).

$$SMA = (SM - SM_{wlt})/(SM_{ref} - SM_{wlt}). \tag{2}$$

Irrigation would be activated if (1) $F_{irr\text{-}crop}$ > IRR_FRC (irrigation fraction threshold, Table 1), (2) the date was during the growing season, (3) SMA < IRR_CRI (SM trigger; Table 1), and (4) precipitation rate < IRR_PCP (a parameter to stop irrigation on rainy days; Table 1).

The growing season was defined in three ways: (1) from planting to maturing stage using IRR_HAR to represent the days before harvesting (Table 1) or (2) as in (1) but using an additional constraint LAI > IRR_LAI (LAI threshold, Table 1) or (3) from planting to maturing stage combined with growing degree days (GDD; Liu et al., 2016) higher than IRR_GDD (GDD threshold; Table 1). In the first method, the input state-level maps of crop-specific planting and harvesting dates were used to determine crop-specific growing season, crucial for crop-specific irrigation modeling. In the third method, the GDD-based growing season enabled the explicit consideration of crop growth stages. Compared to simple use of input-LAI in the second method, calculating GDD at each time step in irrigation modeling allowed for dynamic interactions between crop growth and irrigation.

These criteria were daily checked, and if irrigation was triggered, the potential irrigation amount for that day was computed as the water amount by subtracting the current root-zone SM from the reference point SM_{ref}. The parameter IRR_LIM was used to determine the daily maximum water amount for irrigation, which was mostly associated with irrigation systems (central pivot in this case). Here, it was set to 35 mm as default value based on observations from the irrigated AmeriFlux USNe2 site (see black lines in Figure 6a-6d or Fig. S1 in the supporting information). Therefore, the actual irrigation water amount (IWA, equation (3) below) took the smaller value of (SM_{ref} - SM) and IRR_LIM and would be added to precipitation input at a uniform rate over a prescribed length of time (determined by IRR_LEN and IRR_BEG, Table 1), that is, four hours after 6 a.m. LT as default here similar to Ozdogan et al. (2010) and Leng et al. (2013).

$$IWA = \min(SM_{ref} - SM, \ IRR\_LIM). \tag{3}$$

The above irrigation scheme would be executed for each crop type (if present) in each irrigated grid cell to obtain the irrigation water amount for maize (IWA_{maize}), soybean ($IWA_{soybean}$), winter wheat (IWA_{wheat}), and cotton (IWA_{cotton}), respectively. Finally, the tile-area-weighted grid cell total irrigation water amount (IWA_{tot}) was computed as

Table 2
Design of Field-Scale Numerical Experiments

Experiment	Irrigation parameters	Data used	Objective
CRI0.7	IRR_CRI = 0.7, IRR_LIM = 35, IRR_LAI = 0.0, IRR_FRC = 0.0, IRR_BEG = 6, IRR_LEN = 4, IRR_HAR = 20, IRR_PCP = 1.0	Observed LAI, and planting and harvesting dates	To test the model sensitivity to IRR_CRI
CRI0.6	Same as CRI0.7, but with IRR_CRI = 0.6		
CRI0.5	Same as CRI0.7, but with IRR_CRI = 0.5		
LAI0.0	Same as CRI0.7, but with IRR_CRI = 0.65		To test the model sensitivity to IRR_LAI
LAI0.8	Same as LAI0.0, but with IRR_LAI = 0.8		
LAI1.6	Same as LAI0.0, but with IRR_LAI = 1.6		
GDD0	Same as LAI0.0, but with IRR_GDD criterion instead of IRR_LAI, and IRR_GDD = 0		To test the model sensitivity to IRR_GDD
GDD1	Same as GDD0, but with IRR_GDD = 400		
GDD2	Same as GDD0, but with IRR_GDD = 800		
TCRI0.7 TCRI0.6 TCRI0.5	Same as CRI0.7, CRI0.6, and CRI0.7, respectively	Default LAI, and planting and harvesting dates	To test the model sensitivity to LAI input
TLAI0.0 TLAI0.8 TLAI1.6	Same as LAI0.0, LAI0.8, and LAI1.6, respectively		
TGDD0 TGDD1 TGDD2	Same as GDD0, GDD1, and GDD2, respectively		
TLNoPH0.0 TLNoPH0.8 TLNoPH1.6	Same as TLAI0.0, TLAI0.8, and TLAI1.6, respectively	Default LAI	To test the model sensitivity to planting and harvesting dates
TGNoPH0 TGNoPH1 TGNoPH2	Same as TGDD0, TGDD1, and TGDD2, respectively		
OPTM-LAI	Same as LAI0.0, but with IRR_LAI = 0.0 for maize, and IRR_LAI = 1.5 for soybean	Observed LAI, and planting and harvesting dates	To optimize the field-scale irrigation modeling
OPTM-GDD	Same as GDD1, but with IRR_GDD=0 for maize, and IRR_GDD=650 for soybean		

Abbreviations: GDD, growing degree day; LAI, leaf area index.

$$\begin{cases} \text{IWA}_{\text{tot}} = F_{\text{irr-crop}} \cdot \left(\text{IWA}_{\text{maize}} \cdot F_{\text{maize}} + \text{IWA}_{\text{soybean}} \cdot F_{\text{soybean}} + \text{IWA}_{\text{wheat}} \cdot F_{\text{wheat}} + \text{IWA}_{\text{cotton}} \cdot F_{\text{cotton}} \right), \\ \qquad\qquad\qquad\qquad\qquad\qquad\qquad \text{if } F_{\text{irr}} > F_{\text{crop}} \cdot F_{\text{veg}}; \end{cases} \quad (4)$$

$$\begin{cases} \text{IWA}_{\text{tot}} = F_{\text{irr-crop}} \cdot \dfrac{F_{\text{irr}}}{F_{\text{crop}} \cdot F_{\text{veg}}} \cdot \left(\text{IWA}_{\text{maize}} + F_{\text{maize}} \cdot \text{IWA}_{\text{soybean}} + F_{\text{soybean}} \cdot \text{IWA}_{\text{wheat}} + F_{\text{wheat}} \cdot \text{IWA}_{\text{cotton}} \cdot F_{\text{cotton}} \right), \\ \qquad\qquad\qquad\qquad\qquad\qquad\qquad \text{if } F_{\text{irr}} \le F_{\text{crop}} \cdot F_{\text{veg}}. \end{cases}$$
$$(5)$$

Table 3
Design of Regional-Scale Experiments

Experiment	Irrigation constrain	Irrigation parameters	Data used	Objective
CNTL	Soil moisture deficit plus the growing season determined by planting and harvesting dates	Same as LAI0.0, IRR_CRI = 0.65 for all four crop types	MODIS-based climatology LAI, crop-specific planting and harvesting dates, and crop fractional areas	To serve as a reference run with the calibrated irrigation parameters at the field scale
OPTM2D	Same as CNTL	Same as CNTL, but with calibrated IRR_CRI at the county level	MODIS-based climatology LAI, crop-specific planting and harvesting dates, and crop fractional areas	To obtain a realistic simulation of irrigation water amount at the regional scale
NOIRR	Turn off the irrigation scheme			To serve as a reference run

Abbreviations: LAI, leaf area index; MODIS, Moderate Resolution Imaging Spectroradiometer.
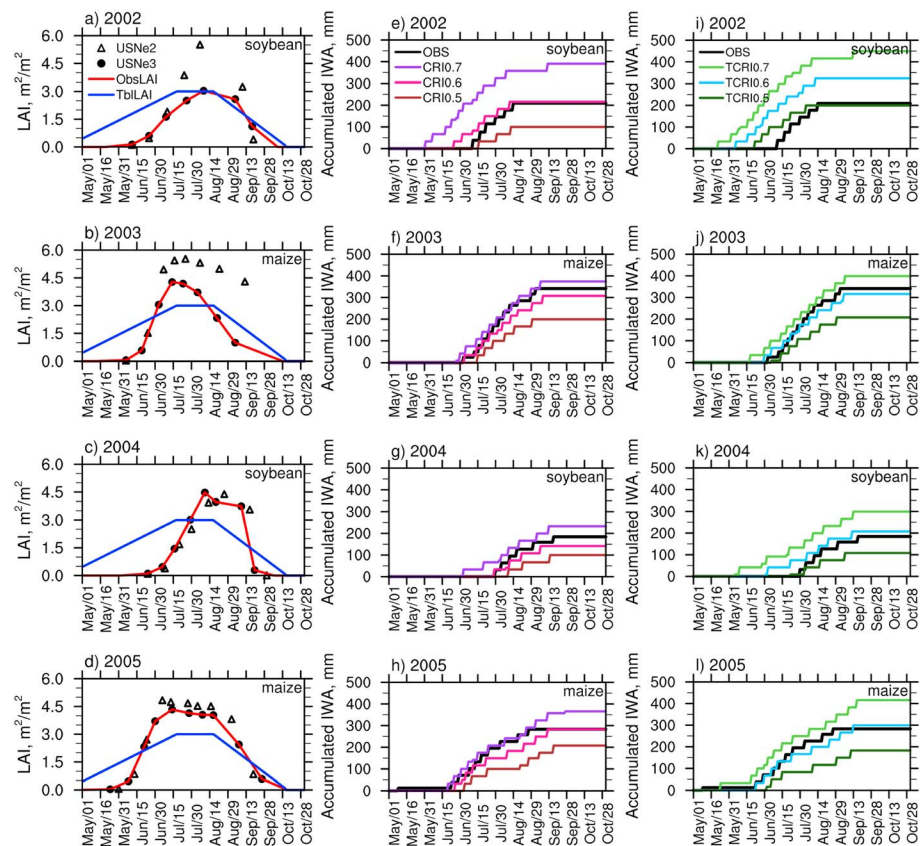
Figure 3. (a-d) Observed (black dots for USNe3 and triangles for USNe2) and default (blue lines) table leaf area index (LAI; unit: m^2/m^2) as model input for 2002-2005. The red lines represent linearly interpolated time series of observed LAI for USNe3. (e-h) Observed (black lines) and modeled (color lines) accumulated irrigation water amount (IWA; unit: mm) for CRI0.7, CRI0.6, and CRI0.5 runs. (i-l) Same as (e)-(h) but for TCRI0.7, TCRI0.6, and TCRI0.5 runs.

2.3. Evaluation Data and Numerical Experiments

2.3.1. Forcing and Evaluation Data

As the first step, field-scale simulations were performed to evaluate the dynamic irrigation scheme and its sensitivities to associated parameters. Such evaluation used measurements from two contrasting agricultural AmeriFlux sites, namely, USNe2 (irrigated, 41°09′53.5″N, 96°28′12.3″W, 362 m) and USNe3 (rainfed, 41°10′46.8″N, 96°26′22.7″W, 363 m) near Mead, Nebraska (see the black star in Figure 1a). Those two sites, within 1.6 km from each other, are located over a flat and relatively homogeneous environment. They are characterized by the same silty-clay-loam soils and undergo the same rotation of maize and soybean. Except for the lower planting density at the rainfed USNe3 site, the only meaningful difference between the two sites for a given year is irrigation (Chen et al., 2018; Verma et al., 2005). More detailed site information can be found in Verma et al. (2005) and Suyker and Verma (2012). The irrigated field (USNe2) is equipped with central-pivot irrigation systems. Most central-pivot provides irrigation water 25-40 mm (1-1.5 inches), and the maximum irrigated water of 35 mm in our analysis was set for IRR_LIM.

Atmospheric forcing conditions were from hourly gap-filled near-surface meteorological data collected at the rainfed USNe3 site. They included air temperature, humidity, pressure, wind speed, downward solar and longwave radiation, and precipitation. The recorded biological data at USNe3, for example, LAI and planting and harvesting dates, were used to define the growing season in HRLDAS. The recorded irrigation applications (including timing and amount; see black lines in Figure 6a-6d or Fig. S1) for the nearby irrigated USNe2 site were used to evaluate the field-scale irrigation modeling.

For regional simulations, we used meteorological forcing conditions derived from the North American Land Data Assimilation System (NLDAS; Cosgrove et al., 2003) forcing dataset at 0.125° and hourly resolutions.

Table 4
The First and Last Irrigation Application Timing (Julian Date) and Total Number of Events for 2002–2005

	2002 (soybean)			2003 (maize)			2004 (soybean)			2005 (maize)		
	First	Last	Total	First	Last	Total	First	Last	Total	First[a]	Last	Total
OBS (USNe2)	192	226	6	184	245	12	212	261	6	174	239	10
OPTM-LAI	190	225	8	182	249	10	203	259	6	174	254	10
OPTM-GDD	190	255	8	182	249	10	213	259	6	174	245	10
CRI0.7	152	255	13	178	249	12	185	257	8	171	270	13
CRI0.6	176	223	7	185	251	10	211	250	5	177	255	9
CRI0.5	197	224	3	196	242	6	223	258	3	185	260	7
TCRI0.7	142	256	16	169	249	12	157	257	11	144	259	13
TCRI0.6	157	224	11	181	248	11	183	256	7	174	256	9
TCRI0.5	173	216	6	187	242	7	204	250	4	183	254	6
LAI0.0	160	225	9	182	249	10	203	259	6	174	254	10
LAI0.8	180	221	7	182	250	11	203	259	6	174	254	10
LAI1.6	191	222	7	182	241	9	202	250	6	174	252	9
TLAI0.0	142	222	12	177	250	11	163	249	8	171	261	11
TLAI0.8	142	222	12	177	250	11	163	249	8	171	261	11
TLAI1.6	157	223	11	177	250	11	163	249	8	171	253	10
TLNoPH0	142	269	13	177	251	12	163	257	9	171	277	12
TLNoPH0.8	142	269	13	177	251	12	163	257	9	171	257	11
TLNoPH1.6	157	223	11	177	250	11	163	249	8	171	253	10
GDD0	160	222	9	182	249	11	203	259	6	174	245	10
GDD1	175	223	8	182	248	11	203	259	6	174	245	10
GDD2	200	222	5	207	250	9	225	258	5	194	256	9
TGDD0	155	222	11	178	250	12	183	250	9	171	248	10
TGDD1	175	222	10	180	246	10	195	258	7	171	245	10
TGDD2	200	222	6	207	248	8	226	259	6	194	244	7
TGNoPH0	155	222	11	178	250	12	183	264	10	171	256	10
TGNoPH1	175	222	10	180	280	11	196	263	8	171	256	11
TGNoPH2	200	222	6	207	248	8	226	259	6	194	244	7

[a]Note that the recorded first irrigation application for 2005 was on 9 May (129 in Julian date), with a relatively low water amount of ~12 mm. The second application was implemented ~45 days later. Thus, the second application timing was used here for the evaluation of modeled irrigation timing.

Precipitation was generated by combining observations from field stations and Stage IV precipitation retrievals from Next Generation Weather Radar Systems and satellites. Initial fields were interpolated spatially and temporally to the NLDAS grid from the North American Regional Reanalysis (NARR; Mesinger et al., 2006). An elevation adjustment was applied to the surface pressure, longwave radiation, and near-surface air temperature and humidity fields to account for discrepancies in topography between the NLDAS and NARR grids.

For regional model evaluation, we used the total freshwater withdrawal data for irrigation at the county level for the year 2000 (Figure 7a below) from the U.S. Geological Survey (USGS; available at https://water.usgs.gov/watuse/data/2000/), which was widely used in irrigation model evaluation (e.g., Leng et al., 2013; Ozdogan et al., 2010).

2.3.2. Experiment Design

To evaluate the performance of the dynamic irrigation scheme as well as its sensitivities to irrigation parameters, a number of field-scale simulations listed in Table 2 were conducted from 15 June 2001 to 31 October 2004. A 10-year spin-up period was used to ensure the SM and temperature reach an equilibrium state. Simulation results for two complete soybean (i.e., 2002 and 2004) and maize (i.e., 2003 and 2005) years were analyzed. The first set of experiments, that is, CRI0.7, CRI0.6, and CRI0.5, were to test the irrigation model sensitivity to the root-zone soil water availability trigger and to obtain a reasonable simulated
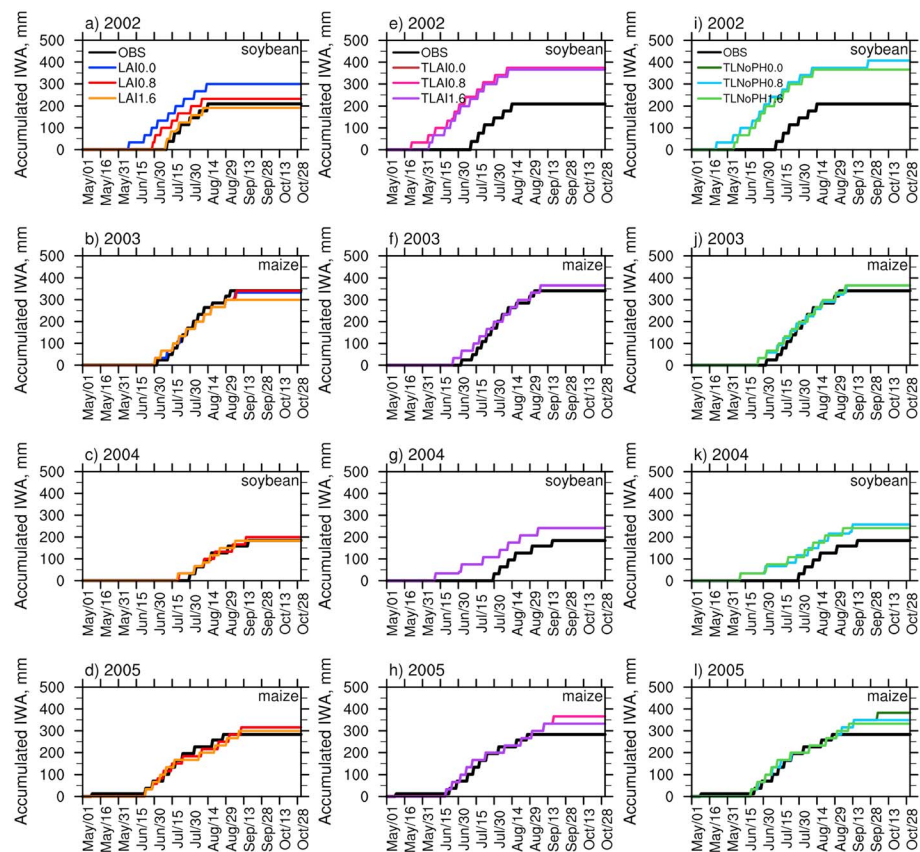
Figure 4. (a-d) Same as Figures 3e-3h but for LAI1.6, LAI0.8, and LAI0.0 runs, unit: mm. (e-h) Same as (a-d) but for TLAI1.6, TLAI0.8, and TLAI0.0 runs, unit: mm. (i-l) Same as (e)-(h), but for TLNoPH1.6, TLNoPH0.8, and TLNoPH0.0 runs, unit: mm.

irrigation amount at the field scale. Two more sets of runs with the LAI-based (i.e., LAI0.0, LAI0.8, and LAI1.6) and GDD-determined (i.e., GDD0, GDD1, and GDD2) growing season were performed to assess impacts of different approach in defining growing season on simulated irrigation. In addition, all the above simulations were repeated with default table LAI values and with or without input planting and harvesting dates. Finally, two optimized runs, that is, OPTM-LAI and OPTM-GDD, were conducted with calibrated irrigation parameters, based on the LAI-determined and GDD-based growing season, which captured well the actual irrigation applications at USNe2.

Regional simulations (see Table 3) were performed from 1 October 1998 to 31 October 2000, with 10-year spin-up periods. Results for the year 2000 were used for model evaluation against the USGS county-level total irrigation withdrawal data (see Figure 7a below). The reference CNTL run was performed with the growing season determined by planting and harvesting dates only, and irrigation parameters were calibrated by field-scale simulations (e.g., IRR_CRI = 0.65 for all four crop types considered here). Considering that the SMA trigger (i.e., IRR_CRI) may vary spatially (Sorooshian et al., 2012), the OPTM2D run employed the county-level calibrated thresholds of IRR_CRI (see text in section 3.2 and Figure 8a below). NOIRR was a reference run for analyzing the modeled effects of irrigation. Note that actual irrigation timing was not available at regional scales, and only the annual total irrigation water amount was evaluated in this study.

3. Results and Discussions

3.1. Field-Scale Irrigation Modeling

In this section, we first examined the roles of different SM trigger criteria in modeled irrigation timing and amount for two complete soybean and maize years. Figures 3a-3d show distinct growth characteristics for those two crops (e.g., peak LAI is reached faster for maize than for soybeans). To quantify the model
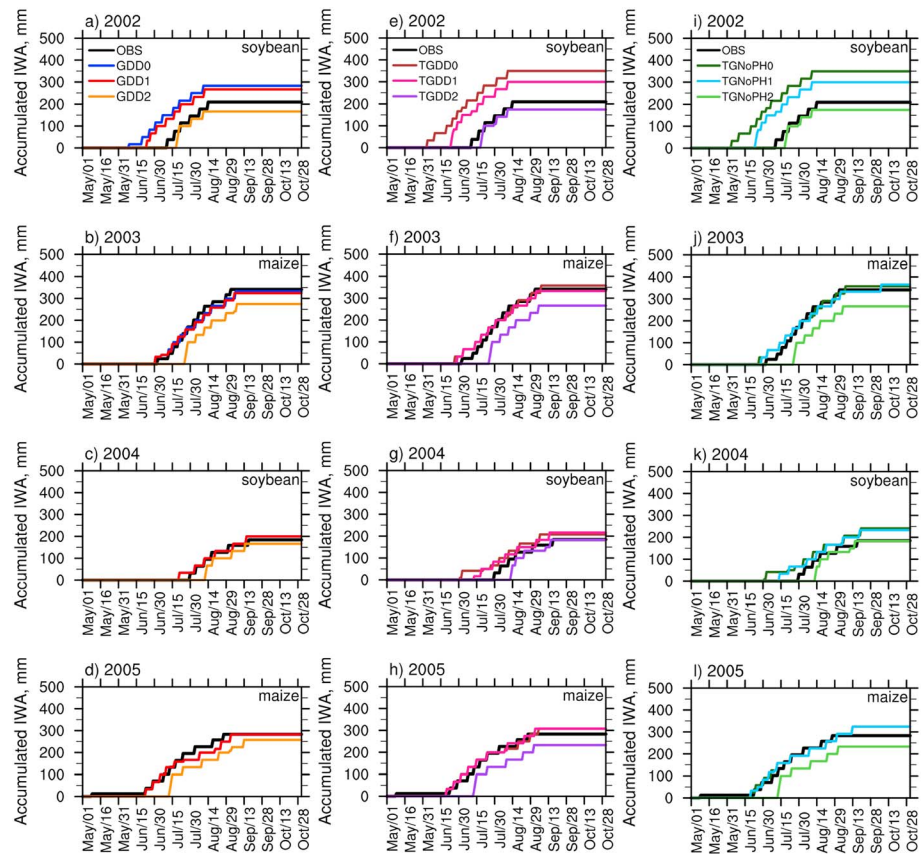
Figure 5. Same as Figure 3 but for simulations with the growing degree day (GDD)-based growing season, unit: mm.

performance in irrigation timing, we analyzed three irrigation features: the total number of applications and dates of the first and last application (Table 4). Note that it usually takes 2-3 days for a center pivot to irrigate the entire crop field.

The root-zone SMA is perhaps the most essential trigger for irrigation. With observed LAI values as model input (red lines in Figures 3a-3d), using IRR_CRI = 0.7 seemed to trigger irrigation too soon for soybean (Figures 3e and 3g) and to overestimate the total irrigation amount for both soybean and maize (Figures 3e-3h). IRR_CRI = 0.6 slightly underestimated the total irrigation water use for 2003 and 2004, although the dates of the first irrigation application were reasonably captured (Figs 3f and 3g). Using IRR_CRI = 0.5, such as in Ozdogan et al. (2010) and Qian et al. (2013), produced delayed dates of the first irrigation application, and significantly underestimated the annual irrigation water amount for the USNe2 site (Figures 3e-3h). Using IRR_CRI = 0.6, compared to the simulation with IRR_CRI=0.7, greatly improved the irrigation timing and shifts the simulated first irrigation application ~25 days closer to observations for soybeans (Figures 3e and 3g and Table 4), but only shifted the first application date slightly for maize about 5 days (Figures 3f and 3h and Table 4). When changing IRR_CRI from 0.7 to 0.5, the modeled first irrigation application was relatively robust for maize, which was likely associated with its faster growing rate than soybeans after seeding (Figures 3a-3d). To obtain an optimal growth, irrigation water demands for maize appear earlier than soybeans, narrowing the timing gap between planting and the first application. Similar trends were also found (Figures 3i-3l) when using default table LAI values (blue lines in Figures 3a-3d), but with larger varying amplitudes for both irrigation timing and total water amount when IRR_CRI changes from 0.7 to 0.5 (e.g., Figures 3k and 3l). Note that all these simulations shown in Figure 3 used actual planting and harvesting dates only to constrain crop irrigation within growing phases.

The growing-season length is another crucial factor for capturing the crop irrigation periods (identified by the first and last application timing). Different methods were used to define the growing season in previous studies, for example, a threshold of 40% of annual range of greenness fraction in Ozdogan
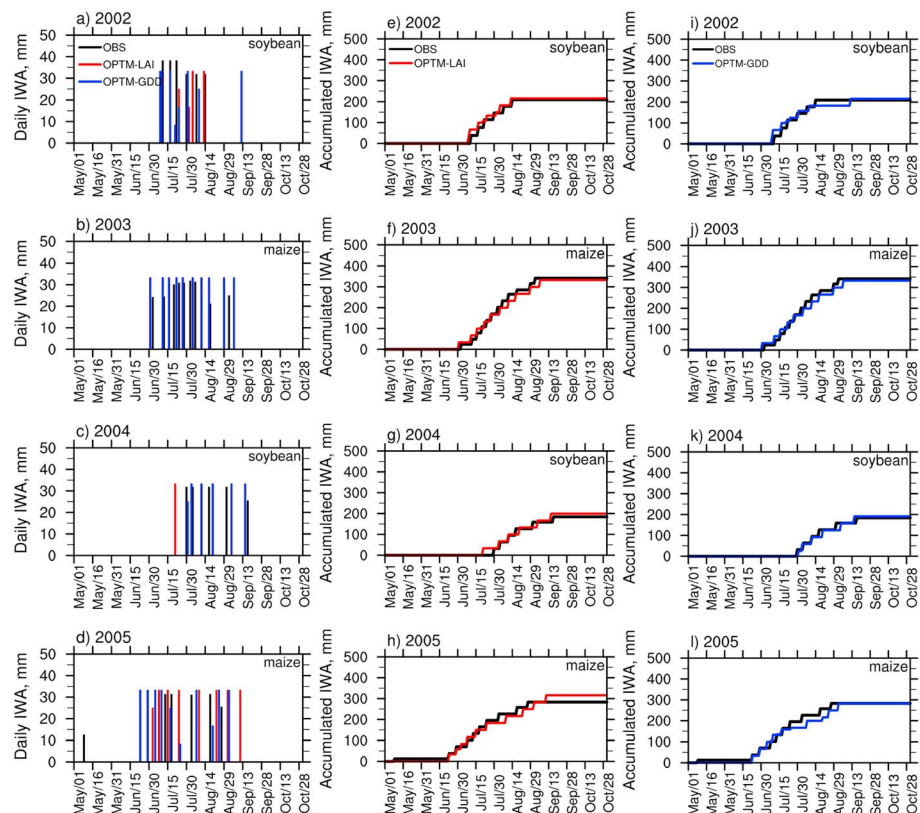
Figure 6. (a-d) Observed (black lines) and modeled (color lines, red for OPTM-LAI and blue for OPTM-GDD) daily irrigation water amount (IWA; unit: mm) for 2002-2005. (e-h) Same as (a)-(d) but for accumulated IWA for OPTM-LAI (unit: mm). (i-l) Same as (e)-(h) but for the OPTM-GDD run (unit: mm).

et al. (2010), and crop leaf area greater than zero in Leng et al. (2013). This study tested three different methods to determine the growing season: from planting to maturing, the LAI threshold, and the GDD threshold; all used IRR_CRI = 0.65 in the following field-scale simulations. Utilizing the LAI threshold (IRR_LAI) ranging from 0 to 0.8 produced a robust performance (Figures 4b and 4d), and both the irrigation timing (see Table 4) and total amount were well captured for the two maize years. For soybean, using planting and harvesting dates only (i.e., IRR_LAI = 0) triggered the first irrigation application too soon (Figure 4a and Table 4), but using the additional LAI constraint (about IRR_LAI = 0.8–1.6) helped mitigate this problem. Nevertheless, Figure 4c shows a less sensitivity of irrigation triggering to LAI threshold values for the relatively wet soybean year 2004, evidenced by the comparable LAI between irrigated and rainfed sites in Figure 3c. Although using default LAI values produces reasonably robust results for maize (Figures 4f, 4h, 4j, and 4l), more realistic LAI input helped correctly identify the growing season and capture the first irrigation timing, especially for soybeans (Figures 4e, 4g, 4i, and 4k and Table 4). The addition of actual harvesting dates helped capture the last irrigation application timing (Figures 4i and 4l and Table 4).

When using the GDD-based growing season, results showed a high sensitivity to the minimum GDD triggering threshold for soybean irrigation over the normal-climate year 2002 (Figures 5a, 5e, and 5i and Table 4). The realistic LAI input seemed to help capture the first application timing for soybean irrigation (e.g., Figures 5c and 5g and Table 4). While for maize years, the dynamic scheme was able to capture well irrigation applications with a GDD threshold greater than zero (Figures 5b, 5d, 5f, 5h, 5j, and 5l and Table 4). In the cases of using the not-so-accurate default LAI, crop-specific GDD triggering thresholds for soybean (IRR_GDD = 400–800) and maize (IRR_GDD = 0–400) helped generate reasonable irrigation simulations (Figures 5e-5h and Table 4). Also, the ending timing for crop irrigation was better captured with actual harvesting dates (Figures 5i-5l and Table 4).
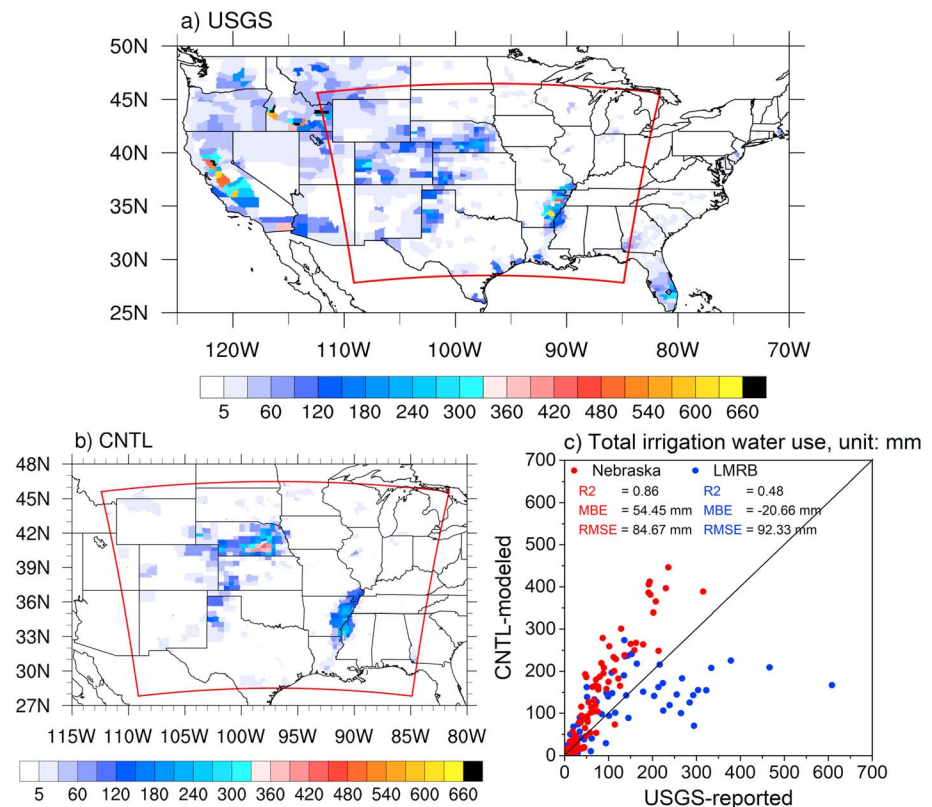
Figure 7. (a) The U.S. Geological Survey (USGS) county-level annual irrigation withdrawals (unit: mm) and (b) total irrigation water amount (IWA) modeled by the CNTL run for the year 2000 (unit: mm). (c) Comparison of the CNTL IWA to the USGS-reported values at the county level. The coefficient of determination (R2), mean bias error (MBE), and root-mean-square error (RMSE) are also presented for Nebraska (red, 93 counties) and Lower Mississippi River Basin (LMRB; blue, 76 counties).

Finally, two simulations, that is, OPTM-LAI and OPTM-GDD, were conducted by respectively utilizing an optimized (i.e., crop-specific) setting of irrigation-model parameters for the LAI-based and GDD-determined growing season, and results are shown in Figure 6. Generally, compared to observations (Figures 2a-2d), both simulations were capable of reasonably capturing the total water amounts for 2002-2005 (Figures 6a-6d), except for a slight overestimation in 2005 by OPTM-LAI (Figure 6h). In terms of irrigation timing, both experiments produced a good estimation of total number of irrigation events (Figures 6a-6d and Table 4). The length of irrigation season (from the first to the last irrigation application) was also well modeled, despite an early shift of ~10 days for the wet soybean year 2004 by OPTM-LAI (Figure 6g). In the OPTM-GDD run, the first application in 2004 and the last application in 2005 were slightly better simulated (Figure 6k-6l and Table 4). In other words, accounting for crop-specific growth seasons is essential in irrigation modeling, especially for soybeans.

The dynamic irrigation scheme in this study was capable of realistically reproducing actual irrigation applications at the field scale, by utilizing crop-specific triggering thresholds to constrain the growing season (e.g., IRR_LAI or IRR_GDD) with irrigation requirements. The actual agriculture management data (e.g., observed LAI and planting and harvesting dates), together with crop-specific irrigation triggers, helped capture both application timing and total water amounts, especially for soybean years.

3.2. Regional-Scale Irrigation Modeling

One great challenge is to transition field-scale irrigation modeling to regional scales. This section discusses the irrigation model performance at regional scale against the USGS county-level total irrigation water withdrawals (Figure 7a). We focused on two heavily irrigated corn and soybean areas (Figures 1b and 7a),
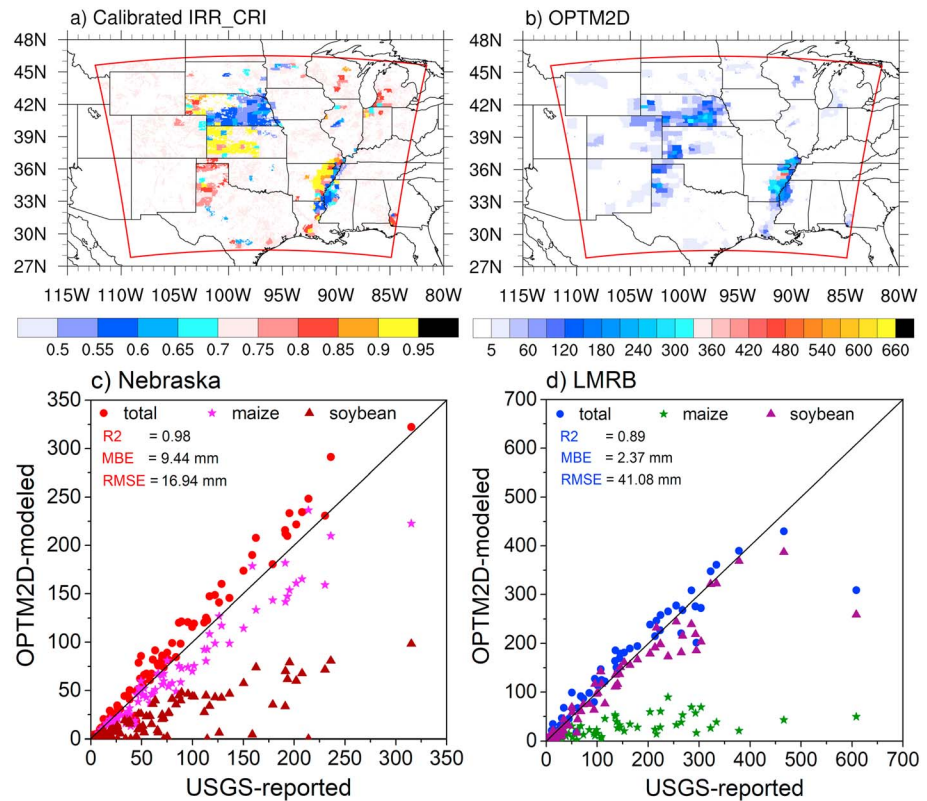
Figure 8. (a) Calibrated IRR_CRI values at the county level over irrigated lands. (b) Total irrigation water amount (IWA; unit: mm) modeled by the OPTM2D run for 2000. The county-level comparison of the OPTM2D-modeled total irrigation water use to the U.S. Geological Survey (USGS)-reported values for (c) Nebraska and (d) Lower Mississippi River Basin (LMRB; unit: mm).

namely, Nebraska in the central plains and LMRB, with the total irrigation water amount peaking around 200–300 mm in southeastern Nebraska and 300–600 mm in eastern Arkansas.

Total IWA simulated by CNTL (Figure 7b), which was heavily constrained by the input irrigation fraction map (Figure 1a), captured well the spatial pattern of the two major irrigated areas. However, compared to the USGS total irrigation withdrawals in Figure 7a, the CNTL run significantly overestimated IWA in southeastern Nebraska and underestimated it in LMRB (Figures 7b and 7c), when using IRR_CRI = 0.65 as in the optimized field-scale simulations. The growing season in CNTL was determined by planting and harvesting dates only (i.e., from seeding to maturing). Several irrigation parameters such as IRR_LIM and IRR_CRI could contribute to these biases. For central-pivot irrigation systems considered in this study, the daily maximum water amount for irrigation (i.e., IRR_LIM) of 25-40 mm plays a limited role in mitigating the model biases of total water requirements. For example, using IRR_LIM = 70 mm (not shown) only increased the modeled total irrigation amount to ~270 mm in eastern Arkansas, where the USGS-reported value was up to 330 mm and even higher (Figure 7a).

The maximum allowable soil-water depletion (i.e., IRR_CRI) depends on both soil type and crop type (Sorooshian et al., 2012), and actual crop conditions and risk level that farmers use to make irrigation decisions. Hence, we calibrated IRR_CRI at the county level by perturbing it between 0.5 and 0.9 at a regular interval of 0.05, similar to the study of Leng et al. (2013) for a weighted factor corresponding to setting the target SM. Figure 8a showed that the calibrated IRR_CRI in southeastern Nebraska is ~0.55, which agreed well with thresholds used in previous studies (e.g., 0.5 in Ozdogan et al., 2010, and Qian et al., 2013); while for LMRB, IRR_CRI was increased to 0.7 or higher in the northwestern part and decreased to ~0.55 in southeastern part. For wheat (ripening), the maximum allowable water depletion was recommended as high as 0.9 by Hanson et al. (2004), consistent with calibrated values in western Kansas (Figure 8a), where winter wheat mainly grows (Figures 1b and 1e). Using calibrated IRR_CRI values in the OPTM2D run produced a better
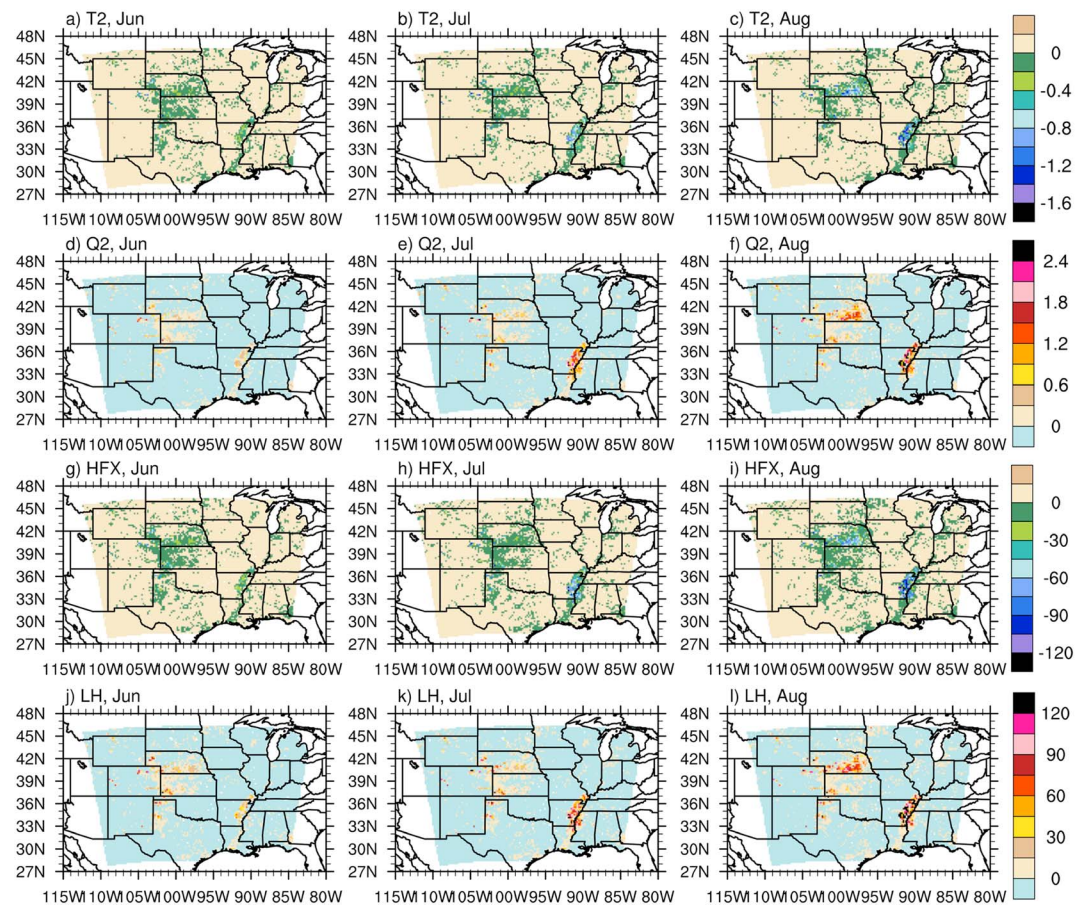
Figure 9. Monthly average changes (OPTM2D minus NOIRR) in (a-c) 2-m air temperature (T2, unit: K), (d-f) 2-m specific humidity (Q2, unit: g/kg), (g-i) sensible heat flux (HFX, unit: W/m^2), and (j-l) latent heat flux (LH, unit: W/m^2) for June, July, and August, 2000.

simulation of total IWA and significantly reduced the overestimations in southeastern Nebraska and underestimations in LMRB with IRR_CRI = 0.65 (Figures 7a and 8b-8d). The coefficients of determination were increased from 0.86 in CNTL to 0.98 in OPTM2D for Nebraska and from 0.48 to 0.89 for LMRB. The mean bias error and root-mean-square error for the OPTM2D run were greatly reduced as well.

Nevertheless, IWA was underestimated for counties in western Colorado, even with IRR_CRI greater than 0.9 (not shown), and such underestimation might be caused by uncertainties in the input irrigation fractional area as pointed out by Leng et al. (2013). Additionally, submerged rice fields with greater irrigation demands were not taken into account in this study, which could be another essential factor contributing to underestimations in some southern irrigated lands (e.g., in eastern Arkansas), and calibrated IRR_CRI values of around 0.9 compensated this deficiency of the irrigation scheme to some extent (Figures 8a, 8b, and 8d). Due to the lack of detailed data sets of irrigation water amounts for each crop type as well as application timing at the regional scale, it is difficult at this stage to further quantify those uncertainties.

Note that although the OPTM2D run captured well total irrigation amounts as in previous studies (e.g., Leng et al., 2013; Ozdogan et al., 2010; Qian et al., 2013), the application timing could be misrepresented at least for soybeans, which required additional LAI or GDD constraints to help locate the first application for soybeans, as indicated by field-scale modeling results (see Figures 4a, 4c, 5a, and 5c). If employing additional constraints, that is, IRR_LAI = 1.5 or IRR_GDD = 650 for soybeans as in optimized field-scale simulations (Figure 6), the OPTM2D run would underestimate the total irrigation amounts in LMRB, where soybean
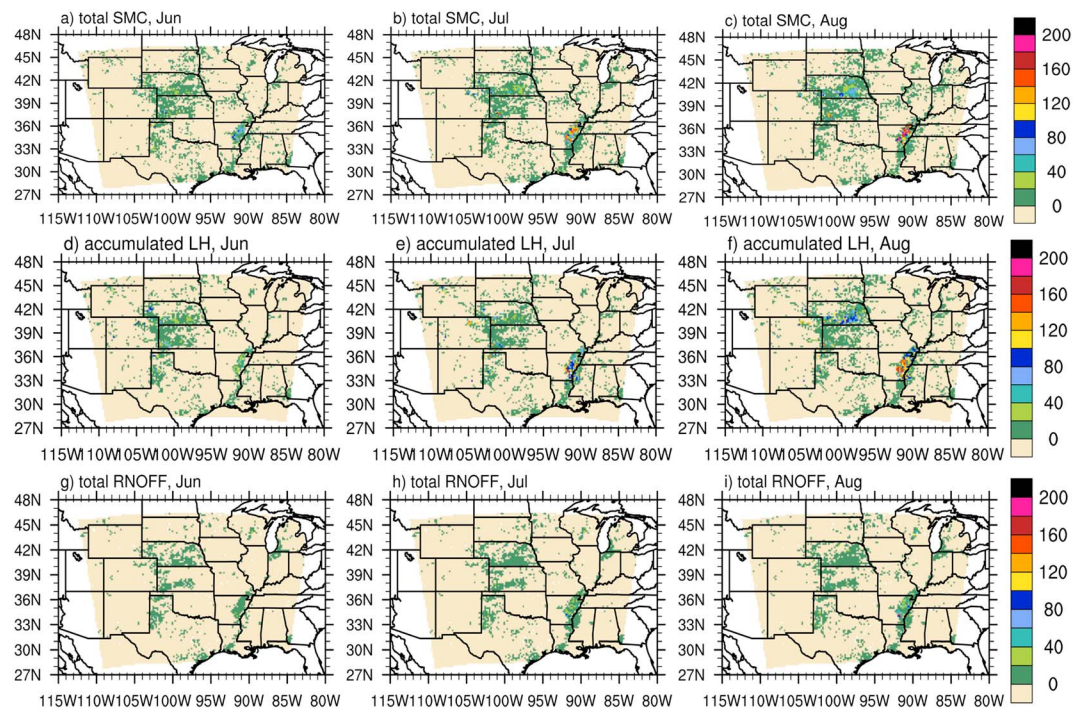
Figure 10. Monthly mean changes (OPTM2D minus NOIRR) in (a-c) total SMC (unit: mm), (d-f), accumulated latent heat (LH; unit: mm), and (g-i) total runoff (unit: mm) for June, July, and August, 2000.

irrigation was dominant (Figures 1b and 1d). Therefore, detailed model evaluation of irrigation timing or crop-specific irrigation amounts are essential for more robust parameter calibrations including IRR_CRI and IRR_LAI or IRR_GDD, and improvements of irrigation modeling when such data sets are available at regional scales.

3.3. Impacts of Irrigation on Surface Hydrometeorology

This section assesses the effects of irrigation on surface hydrometeorological conditions using the OPTM2D run, which simulated reasonably well the total irrigation water by employing calibrated IRR_CRI values, especially in two major irrigated areas. HRLDAS used the lowest model-level (~30m) meteorological conditions from NARR as the atmospheric forcing, so it was possible to diagnose 2-m air temperature and humidity, in addition to the HRLDAS standard output variables such as sensible and latent heat fluxes, and SM.

As demonstrated by many previous studies (e.g., Chen et al., 2018; Cook et al., 2015; Haddeland et al., 2006; Leng et al., 2013; Ozdogan et al., 2010; Pei et al., 2016; Qian et al., 2013; Sacks et al., 2009), irrigation has great influences on land surface water and energy budgets, including the cooling and moistening effects and the repartitioning of sensible and latent heat fluxes shown in Figure9 for the OPTM2D run. In August when the differences between the OPTM2D and NOIRR runs generally reached maxima, the modeled near-surface air temperature decreased by 0.8–1.2 K in southeastern Nebraska and by up to ~1.4 K in eastern Arkansas, while 2-m air humidity increased around 1.2–1.8 g/kg and even greater than 2.4 g/kg over the two above heavily irrigated areas. The degree of cooling or moistening shown here was highly correlated with the total irrigation water amounts (Figures 7a and 8b) and was largely on par with Chen et al. (2018).

Accordingly, the surface energy budget over irrigated regions was also modified (Figs 9g-9l), by shifting sensible heat flux (e.g., a decrease in August of ~60 W/m^2 in southeastern Nebraska and ~105 W/m^2 in eastern Arkansas, respectively) to latent heat flux (e.g., an increase in August of ~75 W/m^2 over southeastern Nebraska and even higher than 120 W/m^2 around eastern Arkansas).
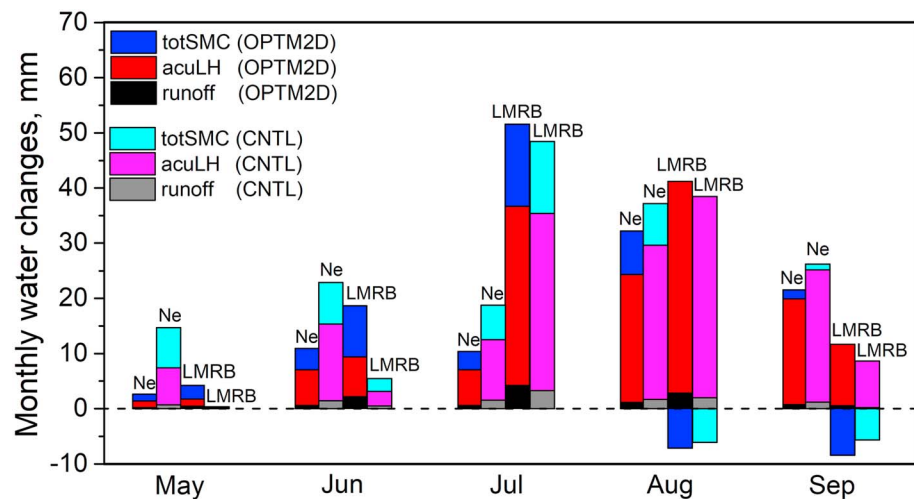
Figure 11. Monthly net changes (OPTM2D or CNTL minus NOIRR, unit: mm) averaged over irrigated grids in Nebraska and Lower Mississippi River Basin (LMRB) for total runoff, accumulated latent heat (LH), and total soil moisture content (SMC) from May to September, 2000.

Moreover, Figure 10 showed the monthly changes in surface water cycle components induced by irrigation. Except for the two heavily irrigated lands in Nebraska and LMRB, irrigation increased summer evaporation, SM storage, and runoff roughly by less than 20 mm. However, in regions with higher irrigation fractions in Nebraska and LMRB, most of irrigation water was used to increase SM and evaporation, rather than runoff. For instance, in August when the cooling and moistening effects of irrigation peaked, the modeled total SMC significantly increased by ~60 mm in southeastern Nebraska and by ~140 mm around eastern Arkansas, respectively (Figures 10a-10c). While the increase in monthly accumulated latent heat flux (i.e., evaporation) was up to ~80 mm in southeastern Nebraska and ~120 mm in eastern Arkansas (Figures 10d-10f).

When averaged over irrigated grids in Nebraska (Figure 11), the OPTM2D-modeled net increases in total SMC were about 3.5 mm (~32% of the total changes in SMC, LH, and runoff) in June and July but rose up to ~7.9 mm (~24% of total water changes) in August. Evaporation was the biggest sink term of irrigation water for Nebraska, about 6–23 mm, contributing to 59–72% of total water changes from June to September. While for LMRB, the net increase in total SMC (~9.3 mm, accounting for ~50% of total water changes) slightly exceeded that for evaporation (~7.2 mm, accounting for ~38% of total water changes) in June. In July and August, evaporation (~35 mm) was the biggest sink term, especially in August when the net change in total SMC was negative. Runoff was the smallest sink term for both irrigated regions, lower than 12% of total water changes in each month. Compared to OPTM2D, the CNTL-produced total water changed greater (smaller) in Nebraska (LMRB), as a result of overestimations (underestimations) of its simulated irrigation amounts.

Figure 12 shows daily-average differences in surface hydrometeorological conditions between simulations by no-irrigation, CNTL, and OPTM2D averaged for Nebraska and LMRB. In terms of irrigation timing, the OPTM2D-modeld first application date was around 18 May in Nebraska (~2 weeks later than the CNTL run) and 28 April in LMRB (~42 days earlier than the CNTL run). The last application dates modeled by the two simulations were comparable. Capturing correctly those first application dates were essential for OPTM2D to better simulate the annual total irrigation amounts. Compared to OPTM2D, the irrigation period (from the first to last application) in the CNTL run was longer (shorter) in Nebraska (LMRB), thus overestimated (underestimated) total irrigation amounts in Nebraska (LMRB). Compared to the USGS-reported total irrigation withdrawals, the CNTL run produced an overestimation of ~55 mm in Nebraska and an underestimation of ~30 mm in LMRB. The cooling and moistening effects induced by irrigation were accordingly overestimated (underestimated) in Nebraska (LMRB) by the CNTL run, as well as the surface energy shift from sensible to latent heat flux. The differences in irrigation timing produced noticeable differences in air temperature, humidity, and surface heat fluxes in May and June.
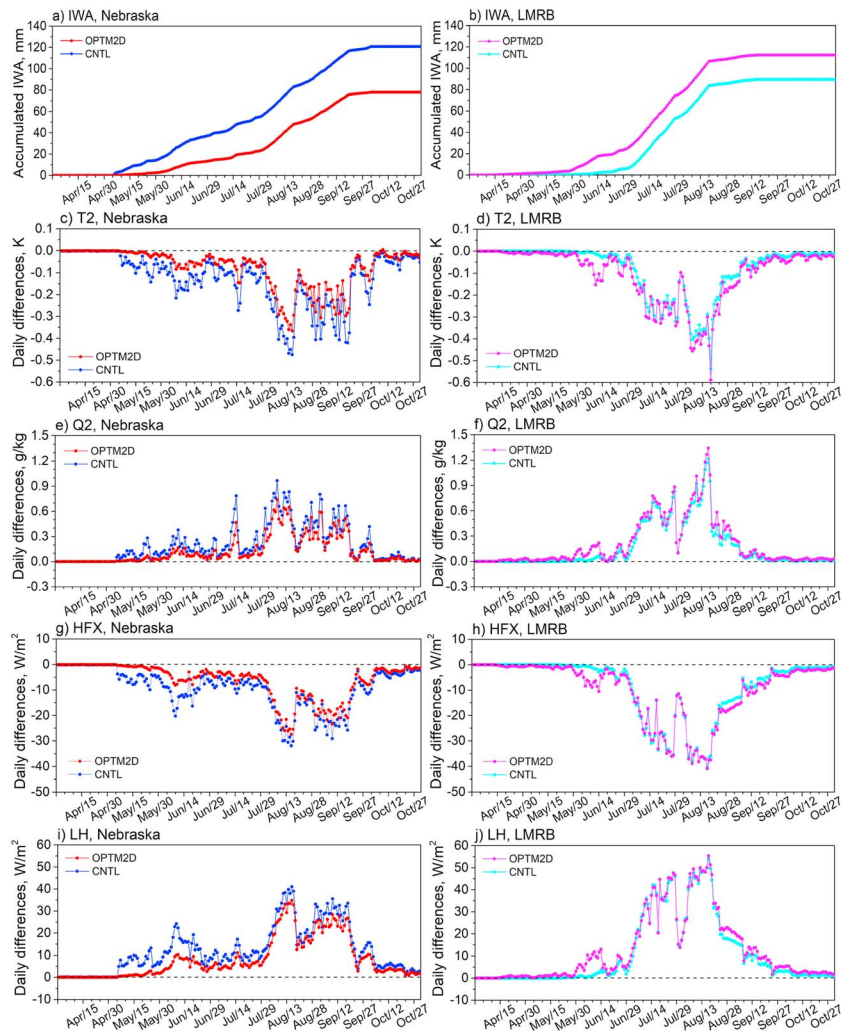
Figure 12. (a and b) Daily accumulated irrigation water amount (IWA, unit: mm) and daily average differences (CNTL or OPTM2D minus NOIRR) in (c and d) T2 (unit: K), (e and f) Q2 (unit: g/kg), (g and h) HFX (unit: W/m^2), and (i and j) latent heat (LH; unit: W/m^2), all of which were averaged over irrigated grids in Nebraska and Lower Mississippi River Basin (LMRB) from April to October 2000.

4. Conclusion and Discussion

The real-world irrigation application is usually crop specific (McDermid et al., 2017), and each type of crop has distinct irrigation timing and water requirements. To mimic these, this study incorporated a dynamic irrigation scheme into the Noah-MP LSM using the root-zone SMA and the growing season as two main irrigation triggers as in previous studies (e.g., Leng et al., 2013; Ozdogan et al., 2010). The unique aspect of this work is to assess the modeling of both the timing and amounts of crop-specific irrigation applications by using various constraints including crop-specific agriculture management data and to highlight the necessity of parameter calibration when transitioning irrigation models from field to regional scales. Compared to Ozdogan et al. (2010) and Leng et al. (2013), this study conducted a systematic validation of the performance of modeled irrigation timing, which is shown to be more substantial at small and subseasonal scales than at large and interannual scales (Lawston et al., 2017). In addition, crop-specific growth stages with different irrigation demands have been taken into account in our scheme but neglected by Ozdogan et al. (2010) and Leng et al. (2013).

A number of field-scale simulations were conducted to understand the general behavior of the dynamic irrigation scheme and its sensitivity to various parameters using observations from two contrasting (i.e.,

irrigated and rainfed) AmeriFlux sites near Mead, Nebraska. Results showed that the irrigation timing and amount for maize and soybeans are different due to their distinct growth characteristics and related water demands. Therefore, using crop-specific triggering thresholds for growing-season length and soil-moisture to constrain irrigation applications was critical for capturing the first application timing and the annual total water amount, especially for soybeans. With a well-calibrated SM triggering threshold of IRR_CRI = 0.65, using the growing season length defined solely by planting and harvesting dates could reasonably reproduce the first irrigation application for maize.

For soybean, however, the additional use of LAI or GDD constraint (e.g., IRR_LAI = 1.5 or IRR_GDD = 650) for defining growing season length was necessary to mitigate an early shift of the modeled first application. More importantly, while the irrigation model could tolerate a certain range of LAI threshold values, realistic LAI input was still crucial for identifying the LAI-based growing season as additional constraint to planting and harvesting dates. When using the GDD-based growing-season approach, actual harvesting dates help determine correctly the timing of the last irrigation.

One great challenge in this study is to transition irrigation modeling from field to regional scales. It is relatively easy to capture the spatial pattern of irrigated regions even with field-scale calibrated soil-moisture triggering threshold, because it is heavily constrained by 500-m MODIS irrigation fraction. However, compared to the USGS county-level irrigation water withdrawals circa 2000, using IRR_CRI = 0.65, significantly overestimated (underestimated) total irrigation amount in southeastern Nebraska (in LMRB). In fact, IRR_CRI depends on both soil type and crop type (Sorooshian et al., 2012), so we calibrated it at the county level following the approach of Leng et al. (2013). The calibrated thresholds agreed well to the values of IRR_CRI from previous studies for maize and soybean (e.g., Ozdogan et al., 2010; Qian et al., 2013) or for winter wheat (Hanson et al., 2004). Even though this study did not explicitly simulate rice crop irrigation, the anomalously high values (e.g., IRR_CRI>0.9) in eastern Arkansas actually reflected the irrigation characteristics of rice fields, which demonstrated the robustness of our calibration procedure. As a result, using calibrated county-level IRR_CRI values significantly mitigated overestimations in southeastern Nebraska and underestimations in LMRB. On the other hand, the input fractional area of irrigated lands could greatly contribute to the general uncertainties in irrigation modeling (Leng et al., 2013).

The land surface hydrometeorological conditions over Nebraska and LMRB were greatly modified by irrigation, including the cooling effect of 0.8–1.4 K, moistening effect of 1.2–2.4 g/kg, reduction in sensible heat fluxes by 60 to105 W/m^2, and increase in latent heat fluxes by 75 to 120 W/m^2. Those local effects were consistent with the observational study by Chen et al. (2018). Note that HRLDAS-simulated irrigation effects concentrated over the irrigated lands due to its offline setting, and future coupling runs with atmospheric models are necessary to improve the understanding of irrigation effects on regional land-atmosphere interactions. For most irrigated regions, the irrigated water was roughly partitioned into increased SM, evaporation, and runoff (less than 20 mm/month). However, in Nebraska and LMRB with higher irrigation fractions, most of irrigation water was used to increase SM and evaporation, rather than runoff.

Overall, it is of importance to use appropriate crop-specific soil-moisture triggers and growing-season length constrained by agriculture management data in reasonably modeling annual total irrigation water demands at regional scales, as in previous studies (e.g., Leng et al., 2013; Ozdogan et al., 2010). Some irrigation parameters such as IRR_CRI are likely dependent of the spatial scales of simulation, as indicated by Iizumi et al. (2014) for parameters in a crop model. The field-calibrated IRR_CRI value was location specific and unrepresentative in regional irrigation modeling, thus causing significant model errors at the regional scale. Future efforts are required to investigate the sensitivity of critical parameters in the irrigation scheme to grid interval. In addition to the model resolution, many other factors, for example, input data sets such as irrigation fraction, irrigation schemes, and parameters used, could also contribute to the uncertainties in modeling irrigation. While regional calibration helps improve model results, a potential over calibration may mask compensate problems caused by lack of presentation of physical processes. For example, flood irrigation over submerged rice fields was not considered in our irrigation scheme, resulting in underestimations in eastern Arkansas in the CNTL run, which was mitigated by IRR_CRI calibration. Hence, there is a need for further model enhancements by incorporating these physical processes and different application methods (Lawston et al., 2015).

Moreover, our irrigation scheme, as demonstrated by field-scale simulations, could capture the crop-specific application timing, a crucial factor but often ignored in previous irrigation modeling studies (Leng et al., 2013; Ozdogan et al., 2010). However, lack of observed irrigation timing and crop-specific parameters at regional scales, transferring the evaluation, and parameter-constraint methods from field to regional scales are very limited for now. For further quantifications of model uncertainties and calibrations of crop-specific parameters (e.g., IRR_LAI and IRR_GDD), it is essential to conduct a detailed evaluation of simulated irrigation amounts and timing (which is now missing) for each crop type at the regional scale when data sets are available. This work showed that detailed agriculture data (e.g., 30-m CropScape and crop-specific planting/harvesting dates) help constrain/improve models. However, transferring this work to a data-scarce region presents challenges, and a strategy for compensating the lack of key data needs to be developed in future work. Future efforts will need to be directed to connecting irrigation water with water resources (e.g., rivers, reservoirs, and groundwater pumping; Leng et al., 2014, 2015, 2017) and evaporative losses (Malek et al., 2017) during irrigation in the context of modeling the full components of water cycle. Since the fundamental purpose of irrigation is to increase crop yields, our future work will focus on evaluating the impacts of irrigation modeling on crop growth and yields (Leng et al., 2016).

References

Bonfils, C., & Lobell, D. (2007). Empirical evidence for a recent slowdown in irrigation-induced cooling. *Proceedings of the National Academy of Sciences*, *104*(34), 13,582–13,587. https://doi.org/10.1073/pnas.0700144104

Boucher, O., Myhre, G., & Myhre, A. (2004). Direct human influence of irrigation on atmospheric water vapour and climate. *Climate Dynamics*, *22*(6-7), 597–603. https://doi.org/10.1007/s00382-004-0402-4

Chen, F., Manning, K. W., LeMone, M. A., Trier, S. B., Alfieri, J. G., Roberts, R. D., et al. (2007). Description and evaluation of the characteristics of the NCAR high-resolution land data assimilation system. *Journal of Applied Meteorology and Climatology*, *46*(6), 694–713. https://doi.org/10.1175/JAM2463.1

Chen, F., Mitchell, K., Schaake, J., Xue, Y., Pan, H. L., Koren, V., et al. (1996). Modeling of land surface evaporation by four schemes and comparison with FIFE observations. *Journal of Geophysical Research*, *101*(D3), 7251–7268. https://doi.org/10.1029/95JD02165

Chen, F., Xu, X., Barlage, M., Rasmussen, R., Shen, S., Miao, S., & Zhou, G. (2018). Memory of irrigation effects on hydroclimate and its modeling challenge. *Environmental Research Letters*, *13*(6), 064009. https://doi.org/10.1088/1748-9326/aab9df

Cook, B. I., Shukla, S. P., Puma, M. J., & Nazarenko, L. S. (2015). Irrigation as an historical climate forcing. *Climate Dynamics*, *44*(5-6), 1715–1730. https://doi.org/10.1007/s00382-014-2204-7

Cosgrove, B. A., Lohmann, D., Mitchell, K. E., Houser, P. R., Wood, E. F., Schaake, J. C., et al. (2003). Real-time and retrospective forcing in the North American Land Data Assimilation System (NLDAS) project. *Journal of Geophysical Research*, *108*(D22), 8842. https://doi.org/10.1029/2002jd003118

de Rosnay, P., Polcher, J., Laval, K., & Sabre, M. (2003). Integrated parameterization of irrigation in the land surface model ORCHIDEE. Validation over Indian Peninsula. *Geophysical Research Letters*, *30*(19), 1986. https://doi.org/10.1029/2003GL018024

Döll, P., & Siebert, S. (2002). Global modeling of irrigation water requirements. *Water Resources Research*, *38*(4), 1037. https://doi.org/10.1029/2001WR000355

Douglas, E. M., Beltrán-Przekurat, A., Niyogi, D., Pielke, R. A. Sr., & Vörösmarty, C. J. (2009). The impact of agricultural intensification and irrigation on land–atmosphere interactions and Indian monsoon precipitation—A mesoscale modeling perspective. *Global and Planetary Change*, *67*(1-2), 117–128. https://doi.org/10.1016/j.gloplacha.2008.12.007

Food and Agriculture Organization (2010). AQUASTAT – FAO's global information system on water and agriculture, FAO, http://www.fao.org/nr/aquastat, last access: 16 March 2010, Rome, Italy.

Gao, Y., Li, K., Chen, F., Jiang, Y., & Lu, C. (2015). Assessing and improving Noah-MP land model simulations for the central Tibetan Plateau. *Journal of Geophysical Research: Atmospheres*, *120*, 9258–9278. https://doi.org/10.1002/2015JD023404

Guimberteau, M., Laval, K., Perrier, A., & Polcher, J. (2012). Global effect of irrigation and its impact on the onset of the Indian summer monsoon. *Climate Dynamics*, *39*(6), 1329–1348. https://doi.org/10.1007/s00382-011-1252-5

Haddeland, I., Lettenmaier, D. P., & Skaugen, T. (2006). Effects of irrigation on the water and energy balances of the Colorado and Mekong river basins. *Journal of Hydrology*, *324*(1-4), 210–223. https://doi.org/10.1016/j.jhydrol.2005.09.028

Hanson, B., Schwankl, L., & Fulton, A. (2004). Scheduling irrigations: When and how much water to apply?, Division of Agriculture and Natural Resources. Pub., vol. 3396, University of California, Davis.

Iizumi, T., Tanaka, Y., Sakurai, G., Ishigooka, Y., & Yokozawa, M. (2014). Dependency of parameter values of a crop model on the spatial scale of simulation. *Journal of Advances in Modeling Earth Systems*, *6*, 527–540. https://doi.org/10.1002/2014MS000311

Kueppers, L. M., Snyder, M. A., & Sloan, L. C. (2007). Irrigation cooling effect: Regional climate forcing by land-use change. *Geophysical Research Letters*, *34*, L03703. https://doi.org/10.1029/2006GL028679

Lawston, P. M., Santanello, J. A. Jr., Franz, T. E., & Rodell, M. (2017). Assessment of irrigation physics in a land surface modeling framework using non-traditional and human-practice datasets. *Hydrology and Earth System Sciences*, *21*(6), 2953. https://doi.org/10.5194/hess-21-2953-2017

Lawston, P. M., Santanello, J. A. Jr., Zaitchik, B. F., & Rodell, M. (2015). Impact of irrigation methods on land surface model spinup and initialization of WRF forecasts. *Journal of Hydrometeorology*, *16*(3), 1135–1154. https://doi.org/10.1175/JHM-D-14-0203.1

Lee, E., Sacks, W. J., Chase, T. N., & Foley, J. A. (2011). Simulated impacts of irrigation on the atmospheric circulation over Asia. *Journal of Geophysical Research*, *116*, D08114. https://doi.org/10.1029/2010JD014740

Leng, G., Huang, M., Tang, Q., Gao, H., & Leung, L. R. (2014). Modeling the effects of groundwater-fed irrigation on terrestrial hydrology over the conterminous United States. *Journal of Hydrometeorology*, *15*(3), 957–972. https://doi.org/10.1175/JHM-D-13-049.1

Leng, G., Huang, M., Tang, Q., & Leung, L. R. (2015). A modeling study of irrigation effects on global surface water and groundwater resources under a changing climate. *Journal of Advances in Modeling Earth Systems*, *7*, 1285–1304. https://doi.org/10.1002/2015MS000437

Leng, G., Huang, M., Tang, Q., Sacks, W. J., Lei, H., & Leung, L. R. (2013). Modeling the effects of irrigation on land surface fluxes and states over the conterminous United States: Sensitivity to input data and model parameters. *Journal of Geophysical Research: Atmospheres*, *118*, 9789–9803. https://doi.org/10.1002/jgrd.50792

Leng, G., Leung, L. R., & Huang, M. (2017). Significant impacts of irrigation water sources and methods on modeling irrigation effects in the ACME L and Model. *Journal of Advances in Modeling Earth Systems*, *9*, 1665–1683. https://doi.org/10.1002/2016MS000885

Leng, G., Zhang, X., Huang, M., Yang, Q., Rafique, R., Asrar, G. R., & Ruby Leung, L. (2016). Simulating county-level crop yields in the conterminous United States using the community land model: the effects of optimizing irrigation and fertilization. *Journal of Advances in Modeling Earth Systems*, *8*, 1912–1931. https://doi.org/10.1002/2016MS000645

Li, J., Chen, F., Zhang, G., Barlage, M., Gan, Y., Xin, Y., & Wang, C. (2018). Impacts of land cover and soil texture uncertainty on land model simulations over the central Tibetan Plateau. *Journal of Advances in Modeling Earth Systems*, *10*, 2121–2146. https://doi.org/10.1029/2018MS001377

Liu, C., Ikeda, K., Rasmussen, R., Barlage, M., Newman, A. J., Prein, A. F., et al. (2017). Continental-scale convection-permitting modeling of the current and future climate of North America. *Climate Dynamics*, *49*(1-2), 71–95. https://doi.org/10.1007/s00382-016-3327-9

Liu, X., Chen, F., Barlage, M., Zhou, G., & Niyogi, D. (2016). Noah-MP-Crop: Introducing dynamic crop growth in the Noah-MP land surface model. *Journal of Geophysical Research: Atmospheres*, *121*, 13953–13972. https://doi.org/10.1002/2016JD025597

Lobell, D., Bala, G., & Duffy, P. B. (2006). Biogeophysical impacts of cropland management changes on climate. *Geophysical Research Letters*, *33*, L06708. https://doi.org/10.1029/2005GL025492

Lobell, D., Bala, G., Mirin, A., Phillips, T., Maxwell, R., & Rotman, D. (2009). Regional differences in the influence of irrigation on climate. *Journal of Climate*, *22*(8), 2248–2255. https://doi.org/10.1175/2008JCLI2703.1

Mahmood, R., Foster, S. A., Keeling, T., Hubbard, K. G., Carlson, C., & Leeper, R. (2006). Impacts of irrigation on 20th century temperature in the northern Great Plains. *Global and Planetary Change*, *54*(1-2), 1–18. https://doi.org/10.1016/j.gloplacha.2005.10.004

Malek, K., Stöckle, C., Chinnayakanahalli, K., Nelson, R., Liu, M., Rajagopalan, K., et al. (2017). VIC-CropSyst-v2: A regional-scale modeling platform to simulate the nexus of climate, hydrology, cropping systems, and human decisions. *Geoscientific Model Development*, *10*(8), 3059–3084. https://doi.org/10.5194/gmd-10-3059-2017

Maupin, M. A., Kenny, J. F., Hutson, S. S., Lovelace, J. K., Barber, N. L., & Linsey, K. S. (2014). Estimated use of water in the United States in 2010. *U.S. Geological Survey Circular, 1405*, 56 pp. https://doi.org/10.3133/cir1405

McDermid, S. S., Mearns, L. O., & Ruane, A. C. (2017). Representing agriculture in Earth System Models: Approaches and priorities for development. *Journal of Advances in Modeling Earth Systems*, *9*, 2230–2265. https://doi.org/10.1002/2016MS000749

Mesinger, F., DiMego, G., Kalnay, E., Mitchell, K., Shafran, P. C., Ebisuzaki, W., et al. (2006). North American regional reanalysis. *Bulletin of the American Meteorological Society*, *87*(3), 343–360. https://doi.org/10.1175/BAMS-87-3-343

National Agricultural Statistics Service (2009). 2007 census of agriculture: Farm and ranch irrigation survey. Vol. 3, Special Studies, Part 1, Rep. AC-070SS-1, National Agricultural Statistics Service, USDA, 268 pp. Retrieved from http://www.agcensus.usda.gov/Publications/2007/Online_Highlights/Farm_and_Ranch_Irrigation_Survey/

National Agricultural Statistics Service (2010). *Field crops: Usual planting and harvesting dates* (Vol. 628). USDA National Agricultural Statistics Service, Agricultural Handbook. Rerieved from https://downloads.usda.library.cornell.edu/usda-esmis/files/vm40xr56k/dv13zw65p/w9505297d/planting-10-29-2010.pdf/

Nazemi, A., & Wheater, H. S. (2015). On inclusion of water resource management in Earth system models - Part 1: Problem definition and representation of water demand. *Hydrology and Earth System Sciences*, *19*(1), 33–61. https://doi.org/10.5194/hess-19-33-2015

Niu, G., Yang, Z., Mitchell, K., Chen, F., Ek, M., Barlage, M., et al. (2011). The community Noah land surface model with multiparameterization options (Noah-MP): 1. Model description and evaluation with local-scale measurements. *Journal of Geophysical Research*, *116*, D12109. https://doi.org/10.1029/2010JD015139

Osuri, K., Nadimpalli, R., Mohanty, U. C., Chen, F., & Niyogi, D. (2017). Improved prediction of severe thunderstorms over the Indian Monsoon region using high resolution soil moisture and temperature initialization. *Scientific Reports*, *7*, 41377. https://doi.org/10.1038/srep41377

Ozdogan, M., & Gutman, G. (2008). A new methodology to map irrigated areas using multi-temporal MODIS and ancillary data: An application example in the continental US. *Remote Sensing of Environment*, *112*(9), 3520–3537. https://doi.org/10.1016/j.rse.2008.04.010

Ozdogan, M., Rodell, M., Beaudoing, H. K., & Toll, D. L. (2010). Simulating the effects of irrigation over the United States in a land surface model based on satellite-derived agricultural data. *Journal of Hydrometeorology*, *11*(1), 171–184. https://doi.org/10.1175/2009JHM1116.1

Pei, L., Moore, N., Zhong, S., Kendall, A. D., Gao, Z., & Hyndman, D. W. (2016). Effects of irrigation on summer precipitation over the United States. *Journal of Climate*, *29*(10), 3541–3558. https://doi.org/10.1175/JCLI-D-15-0337.1

Pokhrel, Y., Hanasaki, N., Koirala, S., Cho, J., Yeh, P. J. F., Kim, H., et al. (2012). Incorporating anthropogenic water regulation modules into a land surface model. *Journal of Hydrometeorology*, *13*(1), 255–269. https://doi.org/10.1175/JHM-D-11-013.1

Pokhrel, Y. N., Hanasaki, N., Wada, Y., & Kim, H. (2016). Recent progresses in incorporating human land–water management into global land surface models toward their integration into Earth system models. *Wiley Interdisciplinary Reviews Water*, *3*(4), 548–574. https://doi.org/10.1002/wat2.1150

Puma, M. J., & Cook, B. I. (2010). Effects of irrigation on global climate during the 20th century. *Journal of Geophysical Research*, *115*, D16120. https://doi.org/10.1029/2010JD014122

Qian, Y., Huang, M., Yang, B., & Berg, L. K. (2013). A modeling study of irrigation effects on surface fluxes and land–air–cloud interactions in the southern Great Plains. *Journal of Hydrometeorology*, *14*(3), 700–721. https://doi.org/10.1175/JHM-D-12-0134.1

Sacks, W. J., Cook, B. I., Buenning, N., Levis, S., & Helkowski, J. H. (2009). Effects of global irrigation on the near-surface climate. *Climate Dynamics*, *33*(2-3), 159–175. https://doi.org/10.1007/s00382-008-0445-z

Saeed, F., Hagemann, S., & Jacob, D. (2009). Impact of irrigation on the south Asian summer monsoon. *Geophysical Research Letters*, *36*, L20711. https://doi.org/10.1029/2009GL040625

Schewe, J., Heinke, J., Gerten, D., Haddeland, I., Arnell, N. W., Clark, D. B., et al. (2014). Multimodel assessment of water scarcity under climate change. *Proceedings of the National Academy of Sciences*, *111*(9), 3245–3250. https://doi.org/10.1073/pnas.1222460110

Shukla, S. P., Puma, M. J., & Cook, B. I. (2014). The response of the South Asian Summer Monsoon circulation to intensified irrigation in global climate model simulations. *Climate Dynamics*, *42*(1-2), 21–36. https://doi.org/10.1007/s00382-013-1786-9

Siebert, S., & Döll, P. (2010). Quantifying blue and green water uses and virtual water contents in global crop production as well as potential production losses without irrigation. *Journal of Hydrology*, *384*(3-4), 198–217. https://doi.org/10.1016/j.jhydrol.2009.07.031

Sorooshian, S., AghaKouchak, A., & Li, J. (2014). Influence of irrigation on land hydrological processes over California. *Journal of Geophysical Research: Atmospheres*, *119*, 13,137–13,152. https://doi.org/10.1002/2014JD022232

Sorooshian, S., Li, J., Hsu, K., & Gao, X. (2011). How significant is the impact of irrigation on the local hydroclimate in California's Central Valley? Comparison of model results with ground and remote-sensing data. *Journal of Geophysical Research*, *116*, D06102. https://doi.org/10.1029/2010JD014775

Sorooshian, S., Li, J., Hsu, K., & Gao, X. (2012). Influence of irrigation schemes used in regional climate models on evapotranspiration estimation: Results and comparative studies from California's Central Valley agricultural regions. *Journal of Geophysical Research*, *117*, D06107. https://doi.org/10.1029/2011JD016978

Suyker, A. E., & Verma, S. B. (2012). Gross primary production and ecosystem respiration of irrigated and rainfed maize–soybean cropping systems over 8 years. *Agricultural and Forest Meteorology*, *165*, 12–24. https://doi.org/10.1016/j.agrformet.2012.05.021

Tuinenburg, O. A., Hutjes, R. W. A., Stacke, T., Wiltshire, A., & Lucas-Picher, P. (2014). Effects of irrigation in India on the atmospheric water budget. *Journal of Hydrometeorology*, *15*(3), 1028–1050. https://doi.org/10.1175/JHM-D-13-078.1

Verma, S. B., Dobermann, A., Cassman, K. G., Walters, D. T., Knops, J. M., Arkebauer, T. J., et al. (2005). Annual carbon dioxide exchange in irrigated and rainfed maize-based agroecosystems. *Agricultural and Forest Meteorology*, *131*(1-2), 77–96. https://doi.org/10.1016/j.agrformet.2005.05.003

Vörösmarty, C. J., Green, P., Salisbury, J., & Lammers, R. B. (2000). Global water resources: vulnerability from climate change and population growth. *Science*, *289*, 284–288. https://doi.org/10.1126/science.289.5477.284

Wisser, D., Fekete, B. M., Vörösmarty, C. J., & Schumann, A. H. (2010). Reconstructing 20th century global hydrography: a contribution to the Global Terrestrial Network-Hydrology (GTN-H). *Hydrology and Earth System Sciences*, *14*(1), 1–24. https://doi.org/10.5194/hess-14-1-2010

Xin, Y. F., Chen, F., Zhao, P., Barlage, M., Blanken, P., Chen, Y. L., et al. (2018). Surface energy balance closure at ten sites over the Tibetan plateau. *Agricultural and Forest Meteorology*, *259*, 317–328. https://doi.org/10.1016/j.agrformet.2018.05.007

Zhang, G., Chen, F., & Gan, Y. (2016). Assessing uncertainties in the Noah-MP ensemble simulations of a cropland site during the Tibet Joint International Cooperation program field campaign. *Journal of Geophysical Research: Atmospheres*, *121*, 9576–9596. https://doi.org/10.1002/2016JD024928